



Quantifying the lowest remnant thickness using a novel broadband wavelength and frequency EMAT utilizing the cut-off property of guided waves

Nived Suresh ^{*}, Krishnan Balasubramaniam

Centre for Non-destructive Evaluation, Department of Mechanical Engineering, Indian Institute of Technology Madras, Chennai, 600036, India

A B S T R A C T

Thickness reduction arising due to corrosion or in any other ways can cause severe damages to structures. Hence regular inspection of structures is vital in many industries. One of the factors deciding the replacement of a structure is the minimum thickness remaining in the structure. A novel ultrasonic method is introduced in this paper to precisely evaluate the minimum remnant thickness of structures. This method utilized the cut-off property of SH1 guided wave mode. A continuous broadband SH1 wave mode was required for establishing this method. This was achieved by exciting a range of wavelength and a range of frequency corresponding to the desired SH1 generation region. The range of wavelength generation was achieved by appropriately selecting the magnet spacings in a Lorentz force EMAT. The range of frequency input was achieved using a linear frequency modulated chirp signal. Finite Element models and experiments were conducted to demonstrate the method. These results are in close agreement.

1. Introduction

Wall thinning is a major concern in many industries, especially in the aerospace and petroleum industries. Corrosion and erosion are some of the main reasons for wall thinning. Tiny defects arising at the beginning, grow over time to become a large defect. These are capable of causing catastrophic failures. Regular inspection is a standard safety procedure that the industries follow, to guarantee the safety of structures.

Guided wave ultrasonic inspection is one of the best-suited methods for corrosion inspection considering the practical implementation limitations. Researchers have extensively worked on these areas to identify defects in plates and pipes. Different wave modes such as Shear Horizontal (SH) modes, Lamb modes, Torsional modes and Longitudinal wave modes were used to characterize defects [1–4]. Most of these techniques use reflection and transmission coefficients to quantify defects. Other than that, there are ways in which time of flight and phase information can be used to measure the extent of defects [5–7].

Apart from these methods, researchers have used the cut-off properties of guided waves to quantify defects. Higher order lamb wave modes such as A1, A2, S1, S2 were successfully used to quantify the defects. Many of the preliminary studies monitored the presence or absence of a particular wave mode to predict whether the minimum remnant thickness is above or below a certain value [8,9]. Researchers also used the shift in peak frequency to measure the remnant thickness

value using the frequency compensation concept [6,9,10]. The success of these methods depends on the identification of the wave mode after it interacts with the defects. Excitation of a single wave mode alone is difficult and the chances of mode conversion from one wave mode to others make these approaches difficult in practical implementations.

Cut-off properties of higher order SH waves were also used to calculate the remnant thickness of structures [11,12]. Belanger et al. utilized higher order wave modes up to SH11. This paper identifies the wave modes that are transmitted through the minimum thickness region. The presence of wave modes and their frequencies is enough to estimate the minimum remnant thickness values in the path of wave propagation. While using higher order wave modes up to SH11, the possibility of mode conversion from one mode to another is higher. While inspecting the defects having a sudden change in thickness, it is also important to consider the study of mode conversion of SH waves [13,14].

SH1 mode alone can also be used to evaluate remnant thickness [15,16]. Implementing this method involves the movement of magnets using intricate mechanisms. The objective is to change the spacing between PPM-EMAT magnets to vary the wavelength of excitation in each experiment. The cut-off frequency found through multiple experiments is sufficient to find the remnant thickness of the structures.

This paper investigates the possibility of finding the remnant thickness by conducting a single experiment utilizing the cut-off property of

* Corresponding author.

E-mail address: nivedkvr@gmail.com (N. Suresh).



SH1 guided wave mode alone. The idea is to generate SH1 wave mode at a range of wavelengths and frequencies in a single excitation. The difference this paper offers from the previous works is the capability of precisely determining the remnant thickness of the structure without any prior calibration data. The accurate determination of thickness helps to guarantee the safety of structures.

Section 2 of this paper discusses the remnant thickness relation to the SH1 cut-off frequency and the excitation wavelength. Section 3 describes how this novel idea is being implemented. Section 4 discusses the Finite Element (FE) simulations for different remnant thickness cases. In section 5, the FE simulations are validated using experiments. This paper concludes with directions for future works.

2. Remnant thickness calculation using cut-off frequency

In this section, the theoretical background of remnant thickness evaluation using cut-off frequency is described. This establishes the need for exciting a broadband signal in terms of wavelength and frequency. The later part of this section describes how broadband excitation in wavelength and frequency is accomplished.

Fig. 1 shows the phase-velocity dispersion diagram for shear horizontal (SH) guided wave modes on an aluminium plate. Only SH0 mode can propagate at all frequency-thickness product values. Higher order modes such as SH1, SH2, etc. exist only after a specific frequency-thickness value. This value above which a wave mode exists is called the cut-off point of that wave mode. As the order of the wave mode increases, the cut-off value increases.

The cut-off value is the product of frequency and thickness. The cut-off frequency is the frequency below which a particular SH wave mode cannot propagate for a given thickness. The cut-off frequency of any SH wave mode in a plate is given by

$$f_{cut-off} = nC_T/2d \quad (1)$$

where $f_{cut-off}$ is the cut-off frequency, n is the order of SH wave mode, C_T is the bulk shear velocity of the plate and d is the thickness of the plate. Similarly, the cut-off thickness is the thickness below which a particular SH wave mode cannot propagate at a given frequency. Cut-off thickness formula can be derived from Equation (1) as

$$d_{cut-off} = nC_T/2f \quad (2)$$

where $d_{cut-off}$ is the cut-off thickness and f is the frequency of the wave mode.

This paper addresses the evaluation of the remnant thickness of

structures utilizing the cut-off properties of SH wave modes. The approach discussed in this paper is theoretically achievable using any higher order SH wave mode. It is, in fact, feasible using any higher order lamb wave modes also. For brevity, we limit our discussions considering the cut-off effect of SH1 wave mode alone.

Fig. 2 depicts the phase velocity dispersion curves for the SH1 wave mode alone at four different thicknesses. As discussed, the SH1 mode at different frequencies has different cut-off thicknesses. It is evident from Fig. 2 that for an SH1 wave mode to travel through a plate of thickness less than 4 mm, the wave mode must possess a frequency higher than 385 kHz. It is also possible to interpret the same idea differently. If the SH1 wave mode at 385 kHz does not propagate through an unknown region of a plate, we can infer that the minimum thickness present in that region is below 4 mm. This is the basic idea of remnant thickness evaluation using the cut-off properties of a single wave mode. Presence of SH1 wave mode at a frequency gives the information that whether the minimum remnant thickness of the inspection region is above or below a specific value. At another frequency, it provides the information regarding another thickness value. Hence performing multiple experiments sweeping a range of frequencies, offers the exact remnant thickness value of the inspection region [15,16].

Consider two 8 mm Aluminium plates, as shown in Fig. 3. This schematic is a cross-section of two dish-shaped defects of different depths. One has the least thickness value of 4 mm and the other has the least thickness value of 6 mm. The radii of defect curvature used in this paper are very high compared to the wavelengths of SH modes. The 4 mm remnant thickness defect has a radius of curvature of 114.5 mm and the 6 mm remnant thickness defect has a radius of curvature of 226 mm. These specific radii of curvature have been chosen to restrict the length of the defect to 60 mm. The cut-off frequency of 4 mm remnant thickness is 385 kHz, and that of 6 mm remnant thickness is 256 kHz. The minimum thickness region in the plate allows the SH1 wave mode to pass through it on only one condition, that is, if the incoming wave mode has a frequency higher than the cut-off frequency of the corresponding minimum thickness value. When SH1 has a frequency lower than the cut-off frequency, the wave mode reflects from the minimum thickness region. Hence the minimum remnant thickness acts as a filter deciding whether the incoming SH1 mode has to reflect or transmit according to its cut-off frequency. Fig. 4 illustrates the relation of the minimum remnant thickness values with the cut-off frequency for SH1 mode in an Aluminium plate. This plot is derived from Equation (2). The markings are the cut-off frequencies of the two remnant thickness cases explained in Fig. 3.

There are certain challenges while employing this method for

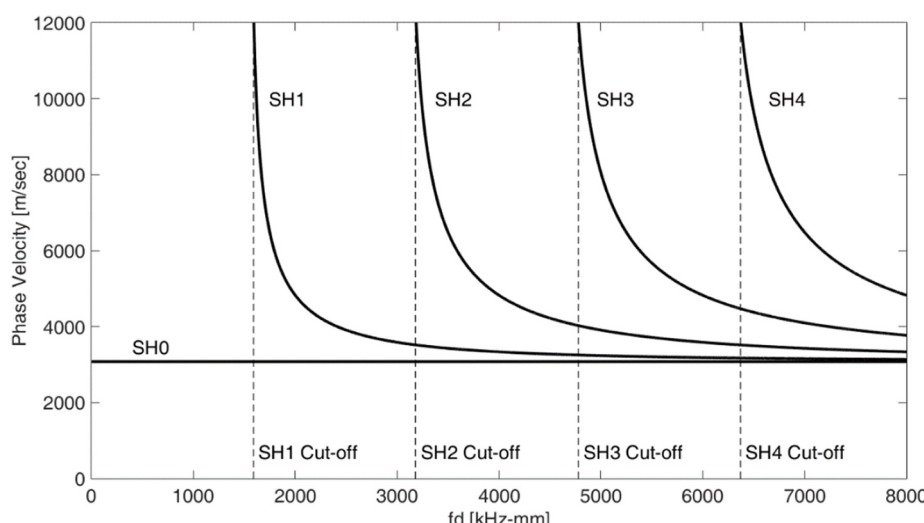


Fig. 1. Phase velocity dispersion curves for SH modes on an Aluminium plate (Bulk shear velocity $C_T = 3128$ m/s).

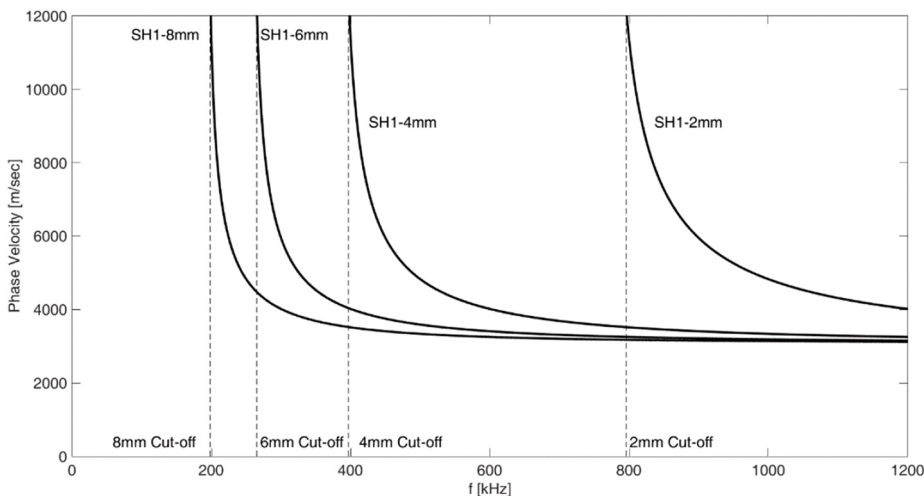


Fig. 2. Phase velocity dispersion curves for SH1 modes at four different thicknesses on an Aluminium plate.

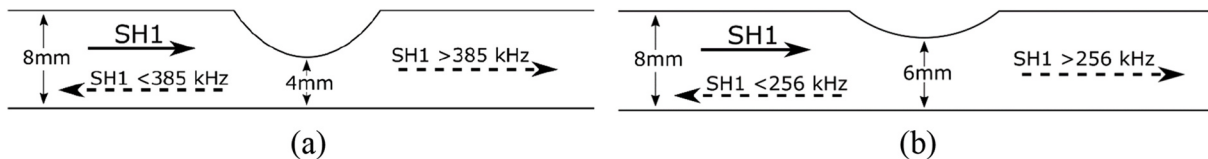


Fig. 3. Dish shaped defects of different depths on an 8 mm aluminium plate (a) 4 mm lowest remaining thickness (b) 6 mm lowest remaining thickness case.

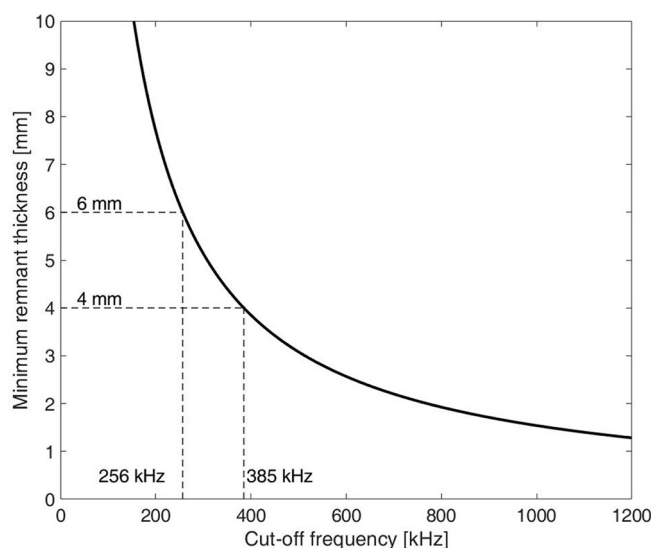


Fig. 4. SH1 mode minimum remnant thickness relation with cut-off frequency for an Aluminium plate.

remnant thickness evaluation. One of them is the mode conversion of SH waves. Researchers have studied the mode conversion from higher order modes to lower order modes, such as SH1 to SH0 [17,18]. Mode conversion can happen from SH0 to SH1 in cases of abrupt change in thickness [13,14]. Even though mode conversion makes remnant thickness evaluation complicated, it is still possible to estimate the remnant thickness value. This paper does not deal with the in-depth analysis of mode conversion since the objective of this paper is to establish a technique to find the remnant thickness. Hence dish-shaped defects are chosen to avoid mode conversions due to abrupt changes in thickness. The authors recognize that further work is required to reliably quantify real corrosion defects.

Another concern is the dispersion effect of the SH1 wave mode. The SH1 wave mode is highly dispersive near the cut-off frequency region. Because of this dispersive nature, the SH1 mode cannot travel as far as a non-dispersive SH0 travels. Even though SH1 is dispersive compared to SH0, the distance considered in this experiment and in many other practical applications are short enough to collect SH1 with sufficient amplitude.

A straight forward way to find the cut-off frequency is by performing multiple experiments, varying the wavelength and frequency of excitation each time [15,16]. The test repeats until the identification of the cut-off frequency. This is a time-consuming process due to the numerous trials to obtain the cut-off frequency i.e. at each location, A-scan data must be acquired for different magnet spacings (i.e. different wavelengths) until the cut-off frequency is found. Also in this approach, there is a requirement of a mechanism to dynamically change the spacing of the magnet. This leads to a relatively long data collection process and consequently a slow rate of scanning of pipes or plates. It is desirable to obtain this information with a single trial in order to improve the speed of inspection.

In this paper, a modified approach to the existing method is considered, simultaneously exciting SH1 at a broad range of both the wavelengths and frequencies in a single experiment. The range in frequency is chosen according to the remnant thickness range to be determined. Thus, a single experiment provides information regarding the remnant thickness of a structure, instead of performing multiple experiments.

3. Broadband SH1 excitation

It is identified that a broadband SH1 wave mode is required to quantify the remnant thickness value in a single experiment. A broadband SH1 wave mode without any break in intensity in between the frequency range is necessary. Otherwise, the frequency at which the band breaks can be wrongly identified as a cut-off frequency. To avoid this false-positive remnant thickness identification, a continuous SH1 wave mode with a considerable amplitude throughout the band is

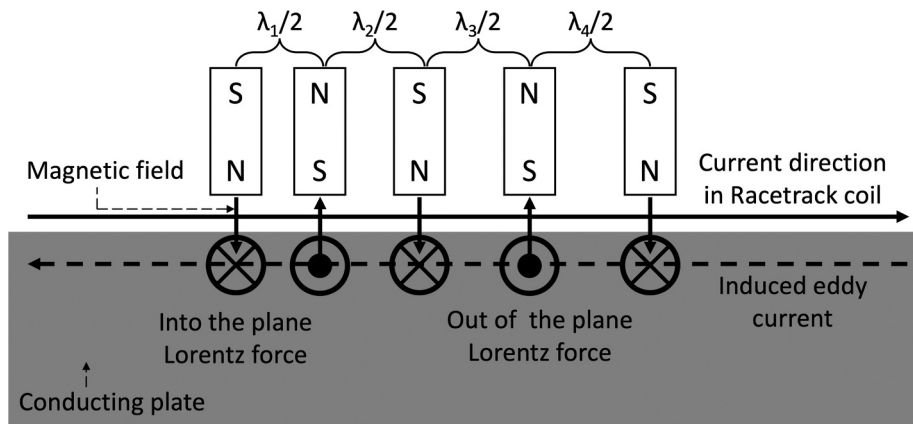


Fig. 5. Lorentz force distribution schematic for generating multiple wavelengths.

essential. Hence, the transduction mechanism should be capable of exciting a range of frequencies of SH1 wave mode without any breaks in any frequencies in between.

Electromagnetic Acoustic Transducers (EMAT) working on the basis of Lorentz force mechanism are selected as transducers, considering their capability of generating SH modes and easiness to work in industrial conditions where non-contact, no-couplant inspection methods are required [19]. For generating SH wave modes researchers have used Periodic Permanent Magnet (PPM) EMAT working on the principle of comb transduction [5,20,33]. In comb transduction, the excitation wavelength is constrained based on the repetition of the source elements. In this paper, a modified form of comb transduction namely Lorentz force EMAT is developed to suit the application. Since the objective here is to excite a range of SH1 wave mode, the excitation wavelength and excitation frequency should be broad enough to accommodate the range.

3.1. Excitation of a broad range of wavelength

Comb transduction in PPM- EMAT is achieved by placing magnets of alternate polarity consecutively. Spacing between the same polarity magnets determines the wavelength of excitation [21]. Hence, by controlling the spacing between magnets, it is possible to control the wavelength of excitation. As a matter of fact, if the number of magnets

increases, coherency in wavelength towards the central wavelength increases. On the contrary, the objective here is not to excite a single wavelength but to excite a range of wavelengths. There are different ways in which a broadband wavelength excitation can be generated. Here the spacing of the magnets is varied to include the contribution of multiple wavelengths. Along with that, the concept of broadband generation by reducing the number of magnets in a PPM-EMAT is also considered. But it is important to make sure that a considerable amount of amplitude is contributed by these wavelengths. Considering the overall size of the transducer, half the wavelength is varied as shown in Fig. 5. Fig. 5 describes how the spacing of the magnets helps to generate Lorentz force at a defined half wavelength. The race track coil is used with current flow in the direction of wave propagation.

To start with, a basic distribution in which wavelength changes linearly over space has been chosen. There are possibilities that some wavelengths do not contribute enough amplitude compared to other wavelengths of excitation. Considering this, magnet positions can be adjusted deviating from the linear arrangement. The contribution of each wavelength can be increased by repeating the spacing of the magnets defining the particular wavelength. This whole arrangement of magnets can be seen as a group of transducers that generate multiple wavelengths at the same time.

The selection of wavelength range is crucial in determining the remnant thickness. The objective here is to determine remnant thickness

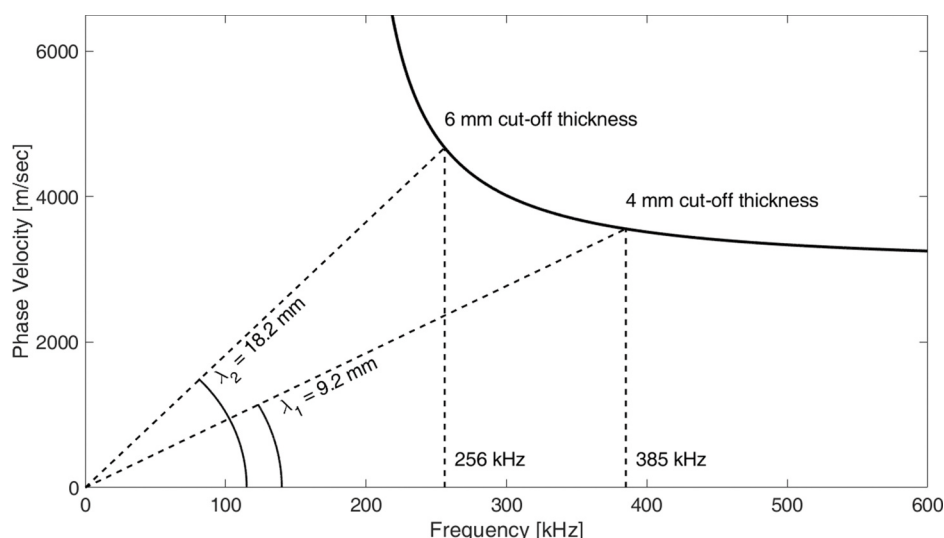


Fig. 6. Phase velocity dispersion curve for SH1 mode alone in an 8 mm Aluminium plate. The frequency and wavelength values for determining 4 mm and 6 mm remnant thicknesses are marked.

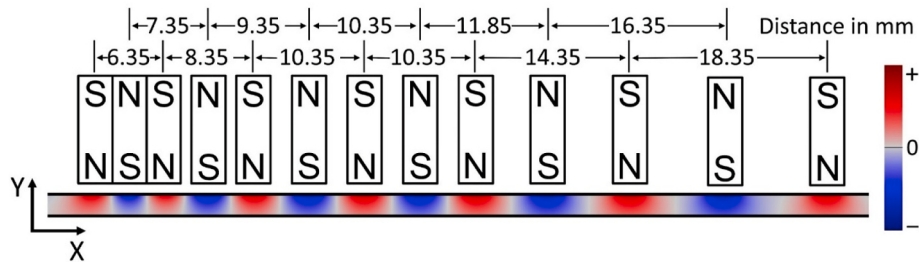


Fig. 7. Magnetic field distribution on the aluminium plate. Wavelength defined using a pair of same polarity magnets is labelled.

of 4 mm, 6 mm and any values in between, on an 8 mm plate as shown in Fig. 3. The cut-off frequency and the excitation wavelength are determined using the dispersion curve of SH1 as shown in Fig. 6. The excitation wavelengths on an 8 mm Aluminium plate to generate the cut-off frequencies for 4 mm and 6 mm remnant thickness are 9.2 mm and 18.2 mm respectively. So, our range of excitation bandwidth should contain the SH1 wave mode having wavelengths from 9.2 mm to 18.2 mm. But it is not recommended to distribute the wavelengths starting from 9.2 mm and ending at 18.2 mm. It is advisable to widen the bandwidth beyond the required range. It is because the determination of remnant thickness does not only consider the transmission of SH1 above the cut-off frequency but also the blockage of SH1 below the cut-off frequency. Hence it is always desirable to increase the required range to a considerable extent.

After determining the range at which the wavelength needs to be excited, the challenging task is to implement this on an EMAT. The wavelength distribution of the Lorentz force is similar to the magnetic field distribution on the plate. Details of wave propagation modelling are described in the next section. The magnetic field distribution on an Aluminium plate is obtained by modelling the arrangement of magnets. To model the magnetic field distribution, a 3D static study in COMSOL Multiphysics [22] is used.

The thickness of the magnet used for modelling is 3.175 mm. This is the thickness with which experiments are conducted. Hence, the minimum wavelength it can produce is 6.35 mm. The upper limit is chosen as 19.35 mm which is above 18.2 mm. The process of finding the positions of magnets started by linearly arranging the magnets according to the wavelength range. In the linear arrangement of magnets, higher wavelengths inherently get higher amplitude contribution because higher wavelengths are integer multiples of lower wavelengths within the range specified. Hence, an additional number of magnets has to be

placed to increase the contribution of lower wavelengths deviating from the linear arrangements of magnets. This way, it is possible to obtain an arrangement of magnets which gives significant amplitudes within the wavelength range specified. It is important to analyse the wavelength contribution by the configuration at each step of the process. It is also significant to limit the number of magnets to the minimum to reduce the size of the probe. The size of the probe in this configuration is 100 mm. A minimum of 13 magnets are required to sufficiently establish the contribution of each wavelength in this case. The final configuration of magnets obtained is shown in Fig. 7.

The wavelength distribution of the Lorentz force is found by collecting the magnetic field in the Y direction on the top surface of the Aluminium plate as shown in Fig. 7. The Y directional component is chosen because the cross product of the magnetic field in the Y-axis with the eddy current in the X-axis results in Lorentz force generation on a plane perpendicular to the X-Y plane, which is the SH wave-particle vibration direction. Fig. 8(a) shows the Lorentz force distribution of the magnet arrangement shown in Fig. 7. In Fig. 8(a), an increase in amplitude while moving towards the higher wavelength region is evident except the regions below the first and last magnets. This is because, when the magnets of opposite polarity come close to each other, the region of the aluminium plate below the magnet gets the effect of positive and negative poles and the intensity reduces. This is why the amplitude increases as the spacing increases. It is obvious that the regions below the first and last magnets deviate from the common trend as these regions do not have magnets on each side. Fig. 8(b) shows the wavelength component present in different configurations of magnet arrangements. In Fig. 8(b), for the variable wavelength plot, although there is a deviation in amplitudes in the contribution of wavelengths between 9.2 mm and 18.2 mm, all these wavelengths contribute a significant amplitude which is sufficient enough to conduct the

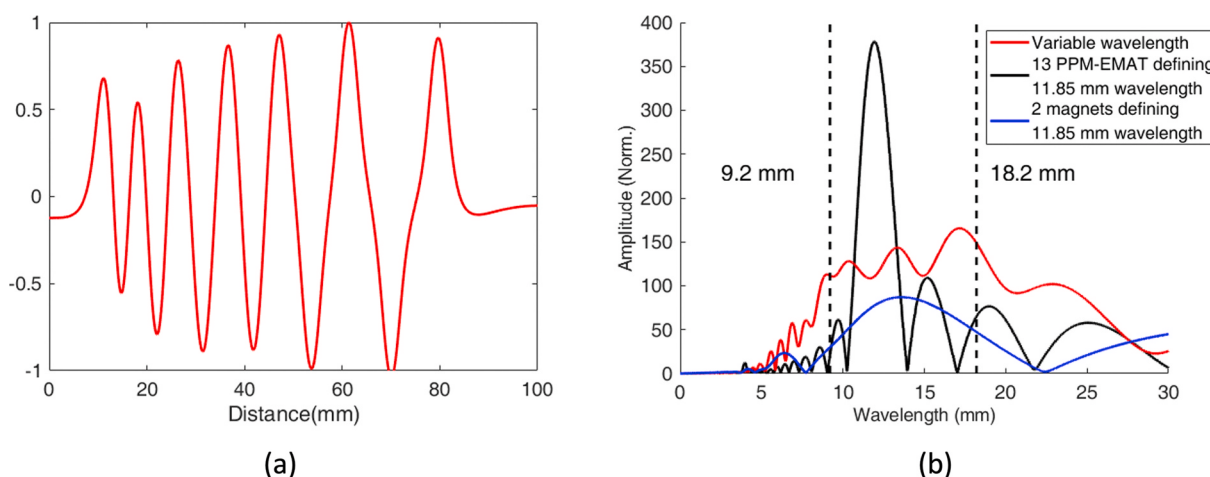


Fig. 8. (a) Magnetic field distribution component in the Y direction on the surface of the aluminium plate (same as Lorentz force distribution) (b) Contribution in terms of wavelengths for three different magnet arrangements.

Table 1

Characteristics of three different magnet arrangements.

	Maximum amplitude (Arb.)	-6dB Wavelength Bandwidth (mm)	Cut-off minimum thickness (mm)	Cut-off maximum thickness (mm)
Broad band excitation	165.55	16.59	3.73	6.742
13 Magnets PPM-EMAT excitation	378.18	2.29	4.50	5.07
2 Magnets excitation	87.02	20.05	4.22	7.05

experiments. To show how the variable wavelength arrangement achieves both better amplitude and broader wavelength simultaneously, two additional plots were plotted. We considered two additional periodic magnet arrangements. These arrangements consisted of 13 and 2 magnets separated by a distance corresponding to 11.85 mm wavelength. It can be easily identified that, PPM-EMAT with 13 magnets defining a wavelength of 11.85 mm has a good amplitude but a poor bandwidth. In addition, 2 magnets arrangement to generate 11.85 mm wavelength has a reasonable bandwidth but low amplitude. **Table 1** quantifies the plots in [Fig. 8\(b\)](#). In addition to the maximum amplitude of each magnet arrangement, its -6dB wavelength bandwidth and range of remnant thickness it can quantify, are also tabulated. It can be inferred that, this arrangement of broad band excitation suits for a thickness evaluation between 4 mm and 6 mm remnant thickness range. For broadband excitation, the bandwidth can be increased by adding additional magnets without the reduction of amplitude.

3.2. Chirp excitation

Broadband frequency signals can be generated in many ways such as spike excitation and chirp excitation. Whichever method is preferred, the response should contain frequency contents within the range as mentioned in [Fig. 3](#), that is, from 256 kHz to 386 kHz. As stated in the previous section, it is required to create a response wider than this frequency range. Linear frequency modulated chirp is used as an excitation signal in this study [23]. It can provide a controlled excitation within the desired range of frequencies. The important quality of the chirp function which suits this application is that the frequency component excited by the chirp signal has almost equal amplitude within the range of excitation frequencies.

The excitation pulse is given in the form of linearly frequency modulated chirp according to the equation given below.

$$f(t) = \sin(2\pi f_0 t + \frac{\pi(f_1 - f_0)t^2}{T}) \quad (3)$$

where f_0 is the starting frequency of excitation, f_1 is the ending frequency of excitation and T is the duration of excitation chirp. The selection of these variables is chosen in such a way that T is minimum and also such

that the required frequency contents have significant amplitudes. To excite the frequencies mentioned with a significant amplitude, f_0 is chosen as 175 kHz and f_1 as 500 kHz for a duration of T , 15 μ s. The linear frequency modulated chirp obtained is shown in [Fig. 9\(a\)](#). [Fig. 9\(b\)](#) shows the frequency contents of the chirp. It is evident that this excitation provides the required frequency contents in a considerable amplitude.

4. Wave propagation modelling

Finite Element Model for wave propagation is developed to study the excitation responses. These excited wave modes are allowed to reflect and transmit through defects described in [Fig. 3](#). After this, 2-D FFT and spectrogram analysis are carried out to identify the wave modes using MATLAB® [24]. These analyses are capable of identifying the cut-off frequency of SH1 wave mode in reflection and transmission.

4.1. Development of model

Wave propagation modelling is performed using the Solid Mechanics module in COMSOL® Multiphysics [22]. It is a 3D time-domain model. The geometry of the model is described in [Fig. 10](#). An aluminium plate of 8 mm thickness is considered. This method of finding remnant thickness will work for other materials such as Steel also. However in magnetic materials such as steel, the magnetostriction effects also need to be considered. Since our model only considers Lorentz force effects, we are limiting the study to non-magnetic materials. Aluminium is chosen here as an example material. The defects in the model have cross-sections as described in [Fig. 3](#). These cross-sections are extruded by 100 mm in Z-axis to create a part of cylindrical gouging defect.

Wave propagation modelling is performed in three different cases. In the first case, a plate without defects is investigated. This helps to confirm the wave modes present in the plate. After this, remnant thickness defects of 6 mm and 4 mm are investigated. Lorentz force distribution is applied at the position marked as Transducer in [Fig. 10](#). This modelling method utilized the magnetic field distribution profile in [Fig. 8\(a\)](#) as the Lorentz force distribution profile on the X-Z plane in the model. Researchers have explored the possibility of replacing the Lorentz body force with an equivalent surface traction. If the eddy current

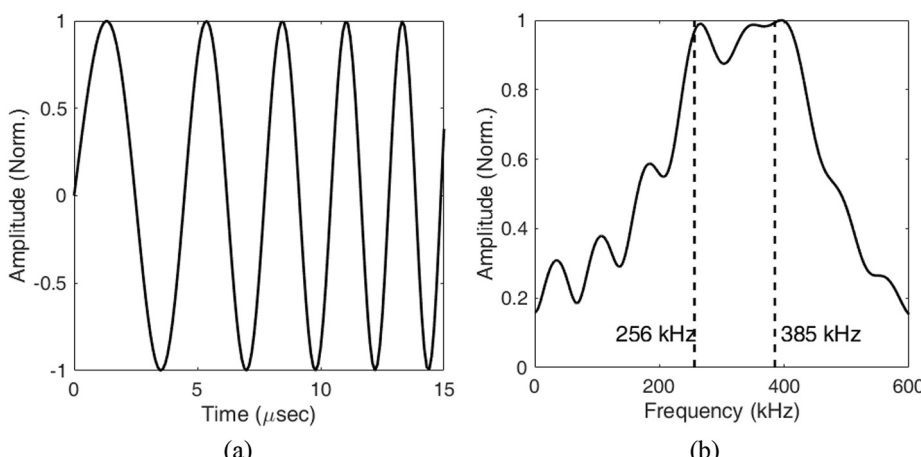


Fig. 9. (a) Linear frequency modulated chirp signal (b) Frequency distribution of the chirp signal.

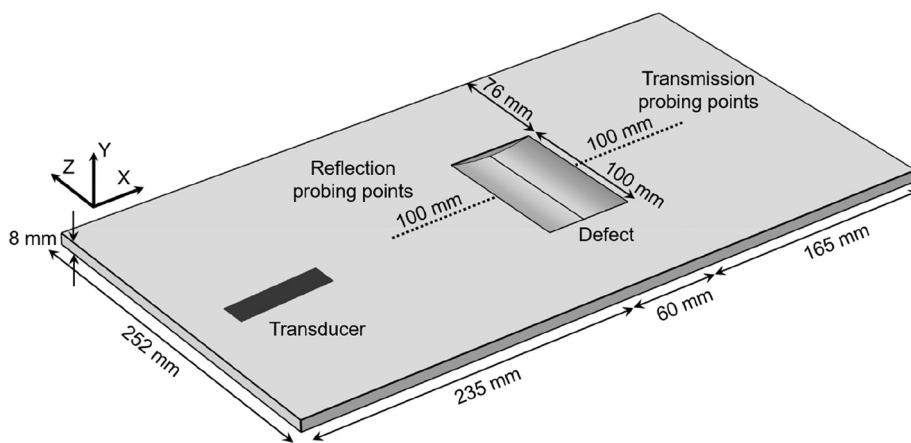


Fig. 10. Schematic of wave propagation modelling and position of probing points.

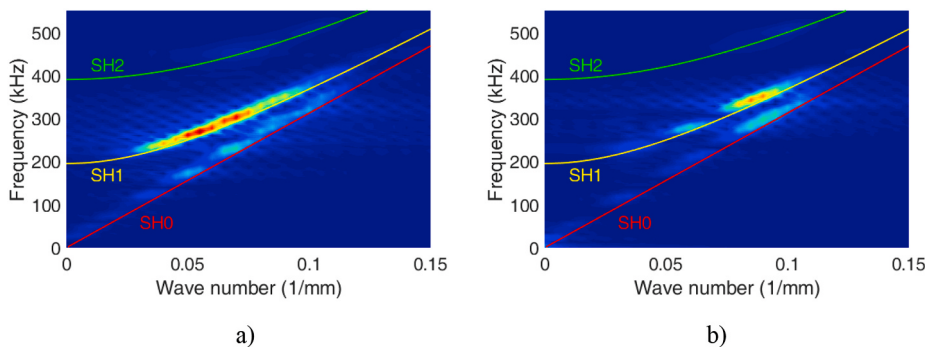


Fig. 11. Modelling 2D-FFT results on a non-defect case using LFM chirp excitation from 175 kHz to 500 kHz and a) variable wavelength excitation from 6.35 mm to 19.35 mm. b) constant wavelength excitation of 10 mm.

skin depth is relatively smaller compared to the acoustic wavelength, equivalent surface stresses can be obtained by integrating the body forces with respect to the depth. Hence, the Lorentz body forces can be treated as effective surface stresses defined by the moments of the body forces [25–29]. The fact is that the existence of equivalent surface traction simplifies the wave propagation modelling. The method proposed for finding the remnant thickness does not require the exact Lorentz force value. It only requires the relative distribution of forces at various wavelengths and frequencies. Hence the Lorentz force distribution profile is considered the same as the magnetic field distribution profile on the surface of the plate, assuming that a constant intensity of eddy-current is generated from the racetrack coil. The direction of the Lorentz force is in the Z-axis. As a result of this, the SH waves get generated in the positive and negative X-axis. Low reflecting boundary conditions are applied throughout the boundaries of the model to avoid unwanted reflections.

Probing points are placed as shown in Fig. 10. Only transmission probing points are considered in the case of the non-defect study. In the case of study with defects, transmission probing points are positioned after the defects, and reflection probing points are positioned before the defects to collect the transmitted and reflected waves respectively.

4.2. Modelling results and discussion

4.2.1. Plate without defects

Fig. 11 illustrates the modelling 2D-FFT [30] results in the plate without defects. The data used to plot this result is a set of A-scans collected at the transmission probing points in the schematic Fig. 10 in the absence of a defect. Data is collected for a length of 100 mm at a gap of 0.5 mm in the positive X-axis direction [31]. Fig. 11 displays only the

positive wavenumber regions of the plot since the study has no interest in the wave travelling in the negative X-axis direction. Theoretical wavenumber-frequency values of SH0, SH1 and SH2 are overlaid to ratify the wave modes. This procedure of generating 2D-FFT has been followed in the forthcoming results also.

The objective of analysing 2D-FFT results in a non-defect case is to show the significance of variable wavelength excitation in finding the remnant thickness. Fig. 11(a) is the modelling 2D-FFT result with variable wavelength and chirp frequency excitation as described before. With these inputs, even though SH0 exists at a minimum amplitude, SH1 is present at a significant amplitude spread within the required frequency range. These results indicate that the wavelength and frequency inputs used are sufficient to calculate the remnant thickness of 4 mm and 6 mm. It is also important to note that there is no break in the intensity of SH1 amplitude over the required range of frequencies.

A PPM-EMAT of constant wavelength is not capable of producing results that the variable EMAT produces. To prove this, the same chirp signal is excited on a 10 mm PPM-EMAT. Fig. 11(b) shows the 2D-FFT results when a PPM-EMAT probe of constant wavelength 10 mm is used. The frequency of excitation used in Fig. 11(b) is the same chirp excitation used in Fig. 11(a). Analysing the results, it can be seen that Fig. 11(b) does not have a continuous SH1 amplitude spread within the required frequency range. It is also evident that Fig. 11(a) has a higher SH1 intensity relative to other wave mode intensities. Hence this leads to the fact that a single PPM-EMAT is not sufficient enough to evaluate the desired remnant thickness. These results show that variable wavelength excitation clearly differs in the ability to produce a continuous broadband SH1 mode exclusively with relatively high intensity. This justifies the selection of variable excitation probe along with chirp excitation in this remnant thickness evaluation process.

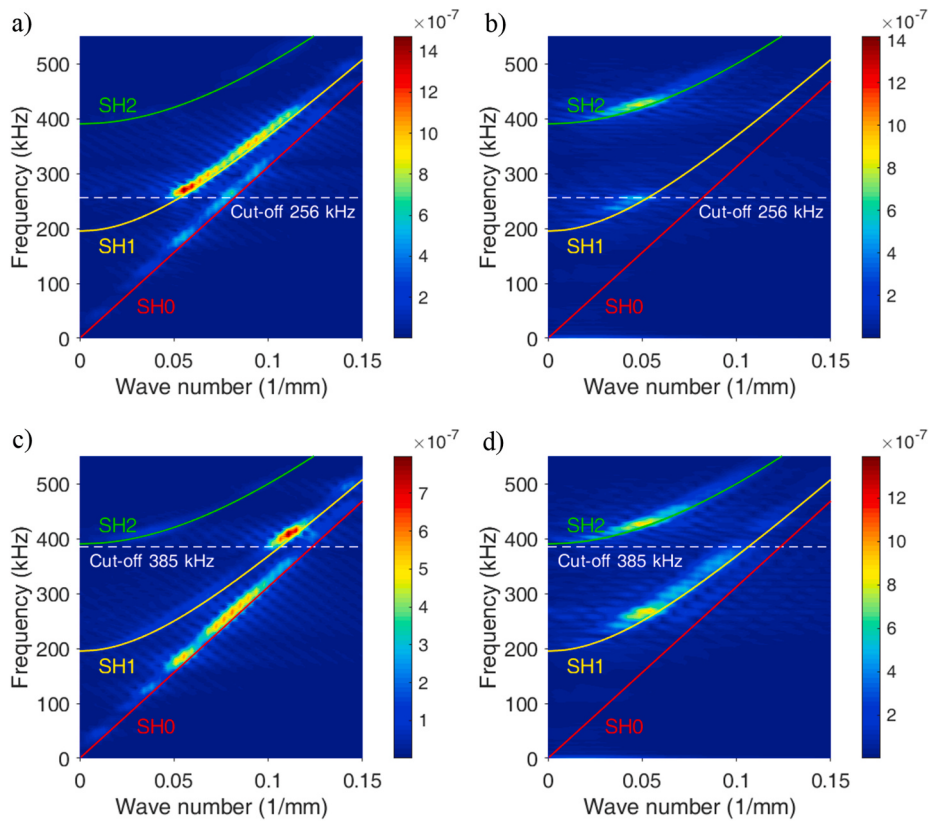


Fig. 12. Modelling 2D-FFT results a) Transmission result of 6 mm remnant thickness defect b) Reflection result of 6 mm remnant thickness defect c) Transmission result of 4 mm remnant thickness defect d) Reflection result of 4 mm remnant thickness defect.

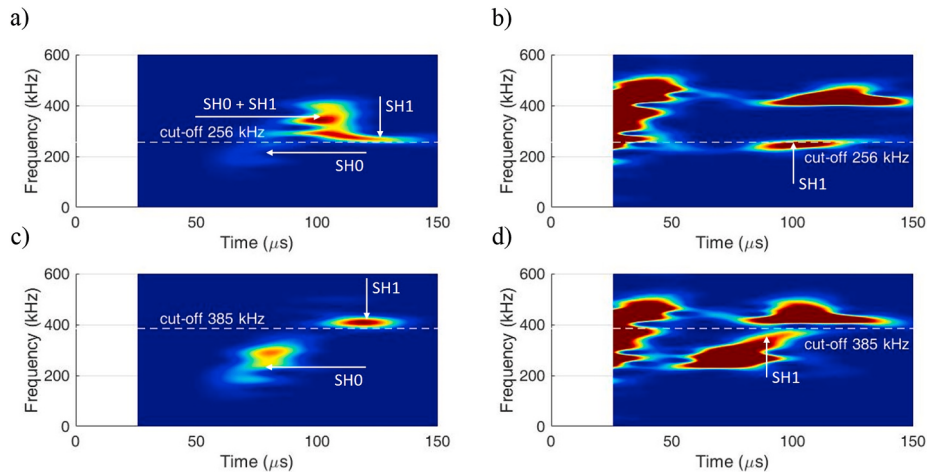


Fig. 13. Modelling Spectrogram results. a) Transmission result on 6 mm remnant thickness defect b) Reflection result on 6 mm remnant thickness defect c) Transmission result on 4 mm remnant thickness defect d) Reflection result on 4 mm remnant thickness defect.

4.2.2. Plate with defects

Fig. 12 shows four different FEM 2D-FFT results of 6 mm and 4 mm remnant thickness defect cases in transmission and reflection. Overlaid dispersion curves allow distinguishing SH1 wave mode from other wave modes.

Fig. 12(a) and **Fig. 12(b)** are the results from the model having a remnant thickness of 6 mm. The cut-off frequency corresponding to 6 mm thickness is 256 kHz which is labelled using a white dotted line. It can be clearly noted that in **Fig. 12(a)** the SH1 amplitude is spread above the cut-off frequency. It is because the 6 mm remnant thickness is not

allowing to transmit the SH1 wave modes having frequencies below 256 kHz. In **Fig. 12(b)** the SH1 amplitude is spread below the cut-off frequency. It is because the 6 mm remnant thickness reflects the SH1 wave modes having a frequency below the cut-off frequency.

Fig. 12(c) and **Fig. 12(d)** can also be interpreted in the same way. These are the results from the model having a remnant thickness of 4 mm. The cut-off frequency corresponding to 4 mm thickness is 385 kHz which is labelled using a white dotted line. It can be clearly noted that in **Fig. 12(c)** the SH1 amplitude is spread above the cut-off frequency. It is because the 4 mm remnant thickness is not allowing to transmit the SH1

wave modes having frequencies below 385 kHz. In Fig. 12(d) the SH1 amplitude is spread below the cut-off frequency. It is because the 4 mm remnant thickness reflects the SH1 wave modes having a frequency below the cut-off frequency.

The presence of SH2 wave mode is evident in the reflection results in Fig. 12(b) and Fig. 12(d). Equation (1) indicates that the cut-off frequency of SH2 is double that of the cut-off frequency of SH1. Hence any SH2 wave mode present below its cut-off frequency reflects back. SH2 wave mode is not present in the transmission results in Fig. 12(a) and Fig. 12(c). It is because SH2 wave mode having a frequency double the cut-off frequency of SH1 only transmits through the defects.

The presence of SH0 wave mode is evident in the transmission results but not in the reflection results. SH0 mode does not have a cut-off frequency; hence it propagates through any thickness. This is why SH0 is present in the transmission results. The reason for the absence of SH0 in the reflection results is because of the shape of the defects. If the defects were not gradual, there is a definite possibility of SH0 reflection [17].

Fig. 13 shows the spectrogram results of the 4 cases discussed in Fig. 12. Here the possibility of obtaining the cut-off frequency from the spectrogram of a single point time response is explored. The intensity in these spectrogram plots are normalised based on the maximum intensity of SH1 wave mode. For transmission results, a probing point 80 mm away from the defect is considered. For reflection results, a probing point 60 mm away from the defect is considered. These probing points are carefully considered making sure that the forward-moving and backward moving waves will not reach the probing point at the same time.

Fig. 13(a) and Fig. 13(c) are the spectrogram plots of the time responses after the wave modes transmitted through the 6 mm and 4 mm remnant thicknesses respectively. The wave mode that appears early in time is the SH0 wave mode. The one arriving after that is the SH1 wave mode. Since these two are transmission results, the lowest frequency present in the SH1 wave mode is identified as the cut-off frequency. The SH0 mode, as expected, is generated over a wide bandwidth of the EMAT. Hence in Fig. 13(c), the SH0 mode separates very well from the SH1 mode. However in Fig. 13(a) SH1 and SH0 are appearing together. This is apparent from Fig. 12(a) and Fig. 12(c) which are the 2D-FFT results for the same. Here we can also observe significant differences in the relative intensities of the SH0 and SH1 modes. The intensity in these plots are normalised based on the maximum intensity of SH1 wave mode.

Fig. 13(b) and Fig. 13(d) are the spectrogram plots of the time responses after the wave modes reflected from the 6 mm and 4 mm remnant thicknesses respectively. The wave modes that appear early in time are the incident wave modes. The wave modes arriving later are the reflected wave modes. SH1 and SH2 wave modes are reflected as shown in Fig. 12(b) and Fig. 12(d). SH1 wave mode is identified by its early arrival time and lower frequency content relative to the SH2 wave mode. The maximum frequency present in the SH1 wave mode is identified as the cut-off frequency.

The cut-off frequency obtained from the spectrogram results are tabulated in Table 2. The remnant thickness value was calculated from the measured cut-off frequency using Equation (2). The resolution in determining the frequency cut-off value using the spectrogram plot, with a digitisation sampling and signal record length used in the experiment, and calculated on the spectrogram plot, is at least 4.879 kHz. This brings a maximum error of 0.1 mm to the 6 mm defect and

0.05 mm to the 4 mm defect.

5. Experimental validation

Experiments were conducted to validate the finite element results. The input parameters used for experiments were the same as those used for FE modelling. Certain modifications had to be implemented in the input chirp signal to accommodate the amplitude variation due to the change in impedance, which will be discussed in the next section. Results were studied using 2D-FFT and spectrogram analysis similar to the FE modelling results.

5.1. Experiment implementation

The first objective was to get a wavelength profile obtained in Fig. 8(a). This was achieved by controlling the spacing between the magnets using acrylic sheets of different thicknesses. Image of the EMAT transducer used for these experiments is shown on the insight of Fig. 14. A multi-turn coil in the shape of a racetrack printed on a flexible PCB was used as the coil of the EMAT transducer. The two rows of magnets on the different sides of the race track coil had opposite polarities so that the Lorentz forces are in the same direction even though the current is in the opposite direction. Agilent arbitrary waveform generator was used to give chirp input waveform to RITEC RPR 4000 as shown in the experiment setup in Fig. 14. In all the experiments, transmitter EMAT remained stationary while the receiver EMAT was moved to all the measurement points indicated in Fig. 10.

RITEC output voltage is proportional to the total impedance of the output circuit. The output circuit had an inductor, the racetrack coil. The impedance of an inductor is proportional to the frequency of the current in that inductor. The frequency in the input chirp varies over time. Hence it results in an impedance change which alters the voltage at the RITEC output terminals. The higher frequency regions in the chirp signal contain higher voltage compared to the lower frequency regions. To compensate for this variation in amplitude, the input LFM chirp amplitude was modified by multiplying with a linear amplitude varying function over time. This resulted in a chirp signal at the output terminal with equal amplitude for all the frequency contents.

RITEC amplified the waveform provided by the Arbitrary waveform generator and sent it to the transmitter EMAT via a $150\ \Omega$ load. A load/electrical termination is a practice of ending the transmission line with a device that matches the characteristic impedance of the line. This is intended to prevent signals from reflecting off the end of the transmission line. A receiver EMAT collected the waveform from the plate and amplified it at the pre-amplifier and sent it to RITEC for further amplification. The final output was displayed on the oscilloscope as shown in Fig. 14.

5.2. Experimental results and discussion

Experimental 2D-FFT results in the transmission and reflection of 6 mm and 4 mm remnant thickness defect cases are shown in Fig. 15.

Fig. 15(a) and Fig. 15(b) are 2D-FFT results from experiments after the wave encountered a remnant thickness of 6 mm. The objective of these plots is to obtain the cut-off frequency corresponding to 6 mm, which is 256 kHz. The frequency at which there is a sudden significant drop in SH1's intensity relative to its surrounding frequency is identified

Table 2

Error in thickness evaluation estimated using numerical spectrogram results.

	Transmission results		Reflection results	
	6 mm remnant thickness	4 mm remnant thickness	6 mm remnant thickness	4 mm remnant thickness
Measured cut-off frequency	256.7 kHz	389.7 kHz	261.05 kHz	378.77 kHz
Calculated remnant thickness	6.00 ± 0.10 mm	3.95 ± 0.05 mm	5.90 ± 0.10 mm	4.06 ± 0.05 mm
Error in thickness evaluation	0%	1.25%	1.6%	1.50%

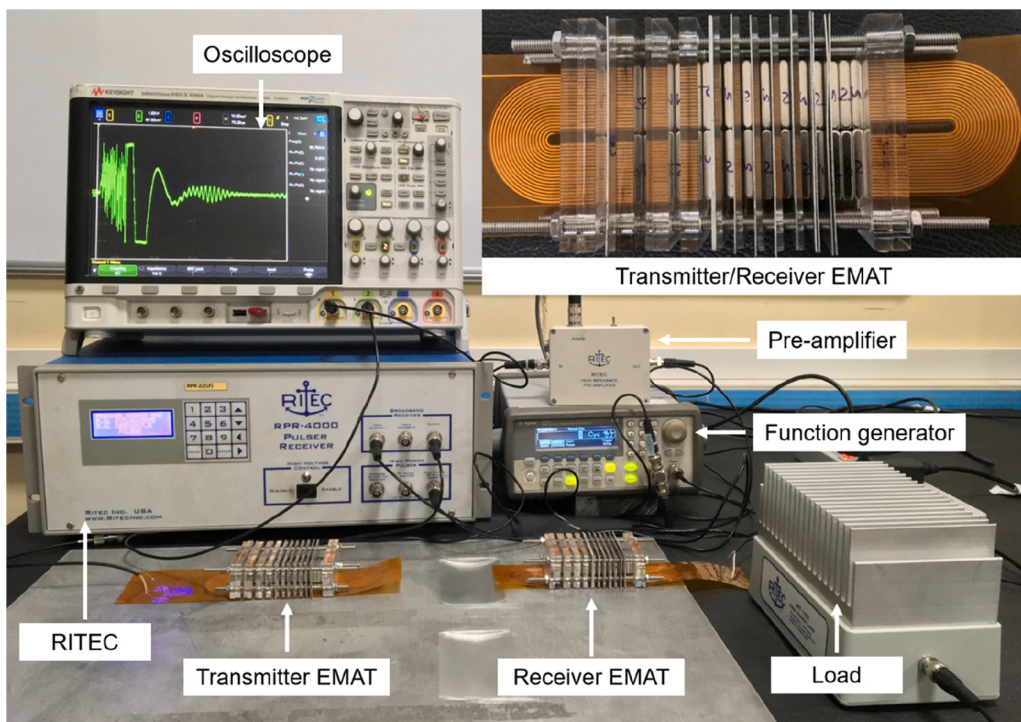


Fig. 14. Experiment setup to evaluate remnant thickness in transmission mode. Transmitter/Receiver EMAT is shown on the insert.

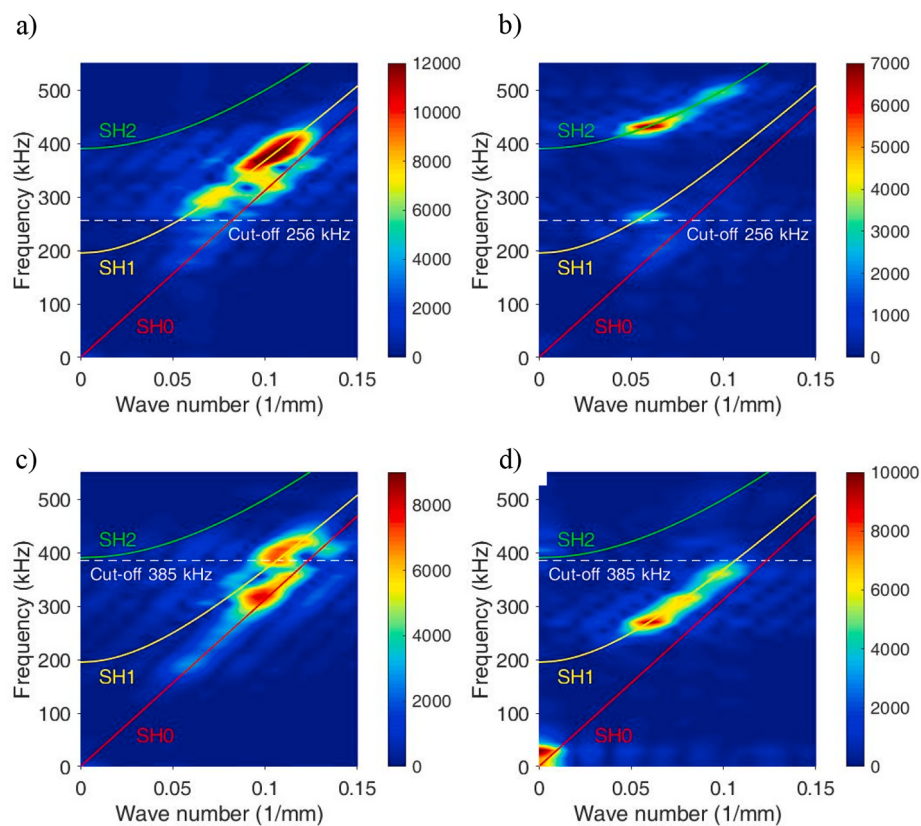


Fig. 15. Experiment 2D-FFT results a) Transmission result of 6 mm remnant thickness defect b) Reflection result of 6 mm remnant thickness defect c) Transmission result of 4 mm remnant thickness defect d) Reflection result of 4 mm remnant thickness defect.

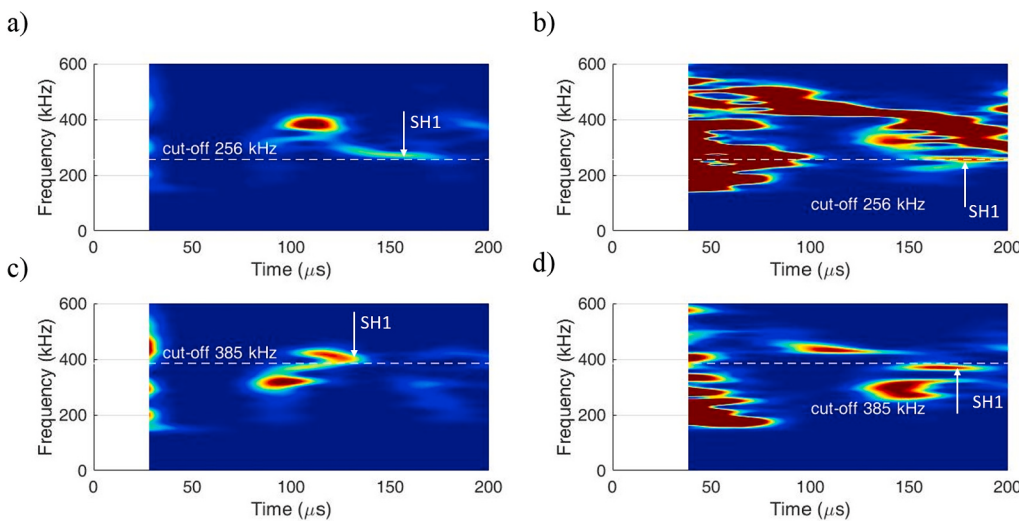


Fig. 16. Experimental Spectrogram results a) Transmission result on 6 mm remnant thickness defect b) Reflection result on 6 mm remnant thickness defect c) Transmission result on 4 mm remnant thickness defect d) Reflection result on 4 mm remnant thickness defect.

Table 3

Error in thickness evaluation estimated using experimental spectrogram results.

	Transmission results		Reflection results	
	6 mm remnant thickness	4 mm remnant thickness	6 mm remnant thickness	4 mm remnant thickness
Measured cut-off frequency	257.4 kHz	381.7 kHz	266.9 kHz	384.1 kHz
Calculated remnant thickness	6.06 ± 0.10 mm	4.08 ± 0.05 mm	5.84 ± 0.10 mm	4.06 ± 0.05 mm
Error in thickness evaluation	1.0%	2.0%	2.66%	1.50%

as the cut-off frequency. The transmission 2D-FFT result, Fig. 15(a), indicates that the cut-off frequency is very close to the original value. But the reflection result, Fig. 15(b), has a higher error when compared to that obtained using the transmission mode.

Fig. 15(c) and Fig. 15(d) are 2D-FFT results from experiments after the wave encountered a remnant thickness of 4 mm. Here the remnant thickness is 4 mm and the cut-off frequency is 385 kHz. The reflection 2D-FFT result, Fig. 15(d), indicates that the cut-off frequency is very close to the original value. But the transmission result, Fig. 15(c), has an error higher than the reflection result.

Fig. 16 shows the spectrogram results of the 4 cases discussed in Fig. 15. Presence of high amplitude noise at the beginning of the reflection results in Fig. 16(b) and Fig. 16(d) is evident. This is arising due to the crosstalk between the EMAT transducers since they are positioned close to each other while receiving the reflected signals. It is not visible in the transmission results, Fig. 16(a) and Fig. 16(c), since the transducers are far apart. The presence of crosstalk masks the direct signal from the transmitter to the receiver. But it does not really affect the analysis since the reflected signals arrive at the receiver after the crosstalk.

The important task is to identify the SH1 wave mode in the spectrogram results. It is fairly easy to identify the SH1 wave modes in the transmission results, Fig. 16(a) and Fig. 16(c), because of the reasons explained in the modelling discussion. Hence the lowest frequency in the transmitted SH1 wave mode can be easily found out. It is a challenging task to identify the SH1 wave mode in the reflection results, Fig. 16(b) and Fig. 16(d). Even though there are many signals present in this case, the highest frequency in the SH1 wave mode still clearly identifies the cut-off frequencies. The analysis becomes easy in the case of large diameter pipes and long plates, since the direct signal from the transmitter and the reflected signal from the defect reach the receiver after a considerable separation in time. SH2 reaches the receiver later in time. Since our focus was on SH1, while plotting spectrogram results for

experiments we did not consider data that larger to include SH2.

After identifying the SH1 wave mode in the spectrogram results, the next objective is to measure the cut-off frequency from it. The lower limit of SH1's frequency is measured from the transmission results. The upper limit of SH1's frequency is measured from the reflection results. An algorithm was developed which picked the highest/lowest frequency, based on the spectrogram intensity values. Primarily, the maximum intensity value of the SH1 wave mode was measured. The cut-off frequency was identified corresponding to an intensity where the intensity value crossed 50% of maximum SH1 intensity. The highest/lowest frequency which crossed this limit was identified as the cut-off frequency and is tabulated in Table 3.

The remnant thickness value was calculated from the measured cut-off frequency using Equation (2). Thickness values obtained were very close to the original thickness values. This method predicted all the remnant thickness values within 2.66% error in transmission and reflection.

6. Conclusion

The cut-off property of SH1 wave mode has been used to measure the lowest remnant thickness. For this method to work, SH1 wave mode needed to be excited in a broad range of both wavelengths and frequencies simultaneously. To achieve this, an EMAT transducer with the variable spacing of magnets capable of producing a wide range of wavelength was used. Along with this, a frequency-modulated chirp excitation generated a broadband SH1 wave mode. FE simulations were used to demonstrate the concept and then it was validated using experiments. Two different defects having remnant thicknesses 6 mm and 4 mm were investigated in reflection and transmission analysis. In experiments, it was shown that a single time response data, upon post-processing, was capable of predicting the remnant thickness with a maximum error of 2.66%. Future work will focus on estimating remnant

thickness having complex geometries such as corrosion in pipelines and shells in a process industry.

Declaration of competing interest

The authors declare that they have no known competing financial interests or personal relationships that could have appeared to influence the work reported in this paper.

CRediT authorship contribution statement

Nived Suresh: Conceptualization, Methodology, Software, Validation, Formal analysis, Investigation, Data curation, Writing - original draft, Writing - review & editing. **Krishnan Balasubramaniam:** Conceptualization, Writing - review & editing, Resources, Supervision, Project administration, Funding acquisition.

Appendix A. Supplementary data

Supplementary data to this article can be found online at <https://doi.org/10.1016/j.ndteint.2020.102313>.

References

- [1] Clough M, Fleming M, Dixon S. Circumferential guided wave EMAT system for pipeline screening using shear horizontal ultrasound. *NDT E Int Mar.* 2017;86 (November 2016):20–7.
- [2] Alleyne DN, Cawley P. The interaction of Lamb waves with defects. *IEEE Trans Ultrason Ferroelectrics Freq Contr May* 1992;39(3):381–97.
- [3] Carandente R, Ma J, Cawley P. The scattering of the fundamental torsional mode from axi-symmetric defects with varying depth profile in pipes. *J Acoust Soc Am Jun* 2010;127(6):3440–8.
- [4] Satyarnarayan L, Chandrasekaran J, Maxfield B, Balasubramaniam K. Circumferential higher order guided wave modes for the detection and sizing of cracks and pinholes in pipe support regions. *NDT E Int* 2008;41(1):32–43.
- [5] Hirao M, Ogi H. An SH-wave EMAT technique for gas pipeline inspection. *NDT E Int Apr.* 1999;32(3):127–32.
- [6] Zhu W, Rose JL, Barshinger JN, Agarwala VS. Ultrasonic guided wave NDT for hidden corrosion detection. *Res Nondestr Eval Jan.* 1998;10(4):205–25.
- [7] Andruschak N, Salettes I, Fillette T, Sinclair A. An NDT guided wave technique for the identification of corrosion defects at support locations. *NDT E Int Oct.* 2015;75: 72–9.
- [8] Silva MZ, Gouyon R, Lepoutre F. Hidden corrosion detection in aircraft aluminum structures using laser ultrasonics and wavelet transform signal analysis. *Ultrasonics Jun.* 2003;41(4):301–5.
- [9] Rose JL, Barshinger J. Using ultrasonic guided wave mode cutoff for corrosion detection and classification. *IEEE Ultrason Symp.* 1998:851–4.
- [10] Tuzzeo D, Lanza Di Scalea F. Noncontact air-coupled guided wave ultrasonics for detection of thinning defects in aluminum plates. *Res Nondestr Eval* 2001;13(2): 61–77.
- [11] Belanger P. High order shear horizontal modes for minimum remnant thickness. *Ultrasonics Apr.* 2014;54(4):1078–87.
- [12] Thon A, Bélanger P. EMAT design for minimum remnant thickness gauging using high order shear horizontal modes. *Ultrasonics May* 2019;95:70–8. March.
- [13] Nurmalia, Nakamura N, Ogi H, Hirao M, Nakahata K. Mode conversion behavior of SH guided wave in a tapered plate. *NDT E Int Jan.* 2012;45(1):156–61.
- [14] Nurmalia N, Nakamura N, Ogi H, Hirao M. Detection of shear horizontal guided waves propagating in aluminum plate with thinning region. *Jpn J Appl Phys Jul.* 2011;50(7):07HC17.
- [15] T. Pialucha, "Transducer for guided wave inspection. Patent number GB 2552858." 2018.
- [16] T. Pialucha, "Determining a thickness of a region of wall- or plate- like structure. Patent number WO 2018/029445 A1." 2018.
- [17] Kubrusly AC, Freitas MA, von der Weid JP, Dixon S. Interaction of SH guided waves with wall thinning. *NDT E Int* 2019;101(May 2018):94–103.
- [18] Kubrusly AC, Freitas MA, von der Weid JP, Dixon S. Mode selectivity of SH guided waves by dual excitation and reception applied to mode conversion analysis. *IEEE Trans Ultrason Ferroelectrics Freq Contr Jul.* 2018;65(7):1239–49.
- [19] Hirao M, Ogi H. EMATs for science and industry. Boston, MA: Springer US; 2003.
- [20] Rose JL, Pelts SP, Quarry MJ. A comb transducer model for guided wave NDE. *Ultrasonics* 1998;36(1–5):163–9.
- [21] Rose JL. Ultrasonic guided waves in Solid media. 2014.
- [22] COMSOL. Documentation for COMSOL release 5.2. COMSOL Inc; 2015.
- [23] Michaels JE, Lee SJ, Croxford AJ, Wilcox PD. Chirp excitation of ultrasonic guided waves. *Ultrasonics Jan.* 2013;53(1):265–70.
- [24] MATLAB. MATLAB:2018. Natick, Massachusetts: The MathWorks Inc.; 2018.
- [25] Kawashima K. Electromagnetic transducer for generation and detection of both longitudinal and transverse ultrasonic waves. Tenn.(USA): Oak Ridge National Lab.; 1975.
- [26] Kawashima K. Theory and numerical calculation of the acoustic field produced in metal by an electromagnetic ultrasonic transducer. *J Acoust Soc Am Nov.* 1976;60 (5):1089–99.
- [27] Thompson RB. The relationship between radiating body forces and equivalent surface stresses: analysis and application to EMAT design. *J Nondestr Eval Jun.* 1980;1(2):79–85.
- [28] Dixon S, a Petcher P, Fan Y, Maisey D, Nickolds P. Ultrasonic metal sheet thickness measurement without prior wave speed calibration. *J Phys D Appl Phys Nov.* 2013; 46(44):445502.
- [29] Seher M, Nagy PB. On the separation of Lorentz and magnetization forces in the transduction mechanism of Electromagnetic Acoustic Transducers (EMATs). *NDT E Int Dec.* 2016;84:1–10.
- [30] Alleyne DN, Cawley P. A 2-dimensional Fourier transform method for the quantitative measurement of Lamb modes. In: IEEE symposium on ultrasonics, vol. 2; 1990. p. 1143–6.
- [31] Le Crom B, Castaings M. Shear horizontal guided wave modes to infer the shear stiffness of adhesive bond layers. *J Acoust Soc Am Apr.* 2010;127(4):2220–30.
- [33] Koodalil Dileep, et al. Detection of interfacial weakness in a lap-shear joint using shear horizontal guided waves. *NDT and E International* 2020. <https://doi.org/10.1016/j.ndteint.2020.102248>.